The Astronomical Journal, 0:1396–1404, 2006 September

THE EFFECTS OF SPACE WEATHERING AT UV WAVELENGTHS: S-CLASS ASTEROIDS

Amanda R. Hendrix
Jet Propulsion Laboratory, California Institute of Technology, MS 230-250, Pasadena, CA 91109; arh@jpl.nasa.gov

and

Faith Vilas[1]
Planetary Astronomy Group, NASA Johnson Space Center/KR, Houston, TX 77058
Received 2006 March 8; accepted 2006 June 1

ABSTRACT

We present evidence that space weathering manifests itself at near-UV wavelengths as a bluing of the spectrum, in contrast with the spectral reddening that has been seen at visible–near-IR wavelengths. Furthermore, the effects of space weathering at UV wavelengths tend to appear with less weathering than do the longer wavelength effects, suggesting that the UV wavelength range is a more sensitive indicator of weathering, and thus age. We report results from analysis of existing near-UV (~220–350 nm) measurements of S-type asteroids from the *International Ultraviolet Explorer* and the *Hubble Space Telescope* and comparisons with laboratory measurements of meteorites to support this hypothesis. Composite spectra of S asteroids are produced by combining UV spacecraft data with ground-based longer wavelength data. At visible–near-IR wavelengths, S-type asteroids are generally spectrally redder (and darker) than ordinary chondrite meteorites, whereas the opposite is generally true at near-UV wavelengths. Similarly, laboratory measurements of lunar samples show that lunar soils (presumably more weathered) are spectrally redder at longer wavelengths, and spectrally bluer at near-UV wavelengths, than less weathered crushed lunar rocks. The UV spectral bluing may be a result of the addition of nanophase iron to the regolith through the weathering process. The UV bluing is most prominent in the 300–400 nm range, where the strong UV absorption edge is degraded with weathering.

Key words: minor planets, asteroids — Moon — ultraviolet: solar system

1. INTRODUCTION

Space weathering, the bombardment of airless bodies by micrometeoroids and irradiation by solar wind particles, affects spectra of solar system bodies by darkening and "reddening" (in which the spectral reflectance increases with wavelength) their surface materials, as well as degrading absorption features (Chapman 1996) at visible–near-IR (VNIR) wavelengths. These effects are well documented for the Moon (e.g., Pieters et al. 1993), where they are apparent in spectra of natural lunar soils, but not seen in spectra of powdered lunar rock samples. The cause of these weathering effects is likely vapor deposition of submicroscopic iron (SMFe; Pieters et al. 2000; Hapke 2001) through solar wind irradiation and micrometeorite bombardment of the lunar surface.

Space weathering is also an important process in the asteroid belt, and is believed to be the cause of spectral differences between ordinary chondrite (OC) meteorites and their proposed parent bodies, S-class asteroids (Chapman 1996; Hapke 2001; Clark et al. 2002a). The VNIR spectral characteristics of weathering of asteroids may be similar to those seen on the Moon (i.e., darkening, red spectral slope, and decreased strength of absorption features). Ratios of *Galileo* SSI camera images of the S-class asteroid Ida in 0.4 and 0.56 μm filters indicate that a number of small, relatively fresh craters are "blue" (increase in reflectance with decreasing wavelength) compared with the reddish rest of the surface, and exhibit stronger 1 μm mafic-silicate absorption bands (Helfenstein et al. 1994; Chapman 1996). Spectral trends with asteroid family age are seen at VNIR wavelengths (Jedicke et al. 2004; Nesvorny et al. 2005), consistent with lunar-like space weathering. The source of asteroid weathering effects is under debate: Hapke (2001) suggested that SMFe is deposited through solar H ion bombardment or through micrometeoroid impacts, as the addition of SMFe-bearing coatings to the grains of an OC meteorite sample results in spectral reflectance features similar to those of an S-class asteroid. Others (e.g., Strazzulla et al. 2005) have shown that heavy ion bombardment produces weathering effects in asteroid weathering simulations through the formation of cation displacements. Brunetto & Strazzulla (2005) suggest that sources of weathering among asteroids may vary with solar distance, with heavy ion bombardment having the greatest effect in the inner solar system (for near-Earth objects) and micrometeoroid impacts being dominant in the main belt. Near-Earth objects have been found to display a trend between size and spectral slope (Binzel et al. 2004), suggestive of space weathering effects; Marchi et al. (2006) used a data set of S-class asteroids near Earth and the main belt and found a slope-distance relationship consistent with a solar source of weathering.

The effects of space weathering at UV wavelengths have not previously been well studied. In this report we first outline previous work suggesting that the manifestation of space weathering in the UV is a spectral bluing. We then present results of a new analysis of UV spectra of S-type asteroids to supplement this theory.

2. BACKGROUND: PREVIOUS RESULTS

Recent evidence indicates that the UV-visible wavelength region is very sensitive to even small amounts of weathering. The effects of space weathering at UV–visible wavelengths include a bluing of the spectral reflectance and, in some cases, a spectral reversal (in which visibly relatively dark surfaces are relatively bright at shorter wavelengths). As explained below, these effects are displayed in lunar samples, laboratory spectra of lunar samples,

[1] Current address: MMT Observatory, University of Arizona, P.O. Box 210065, Tucson, AZ 85721.

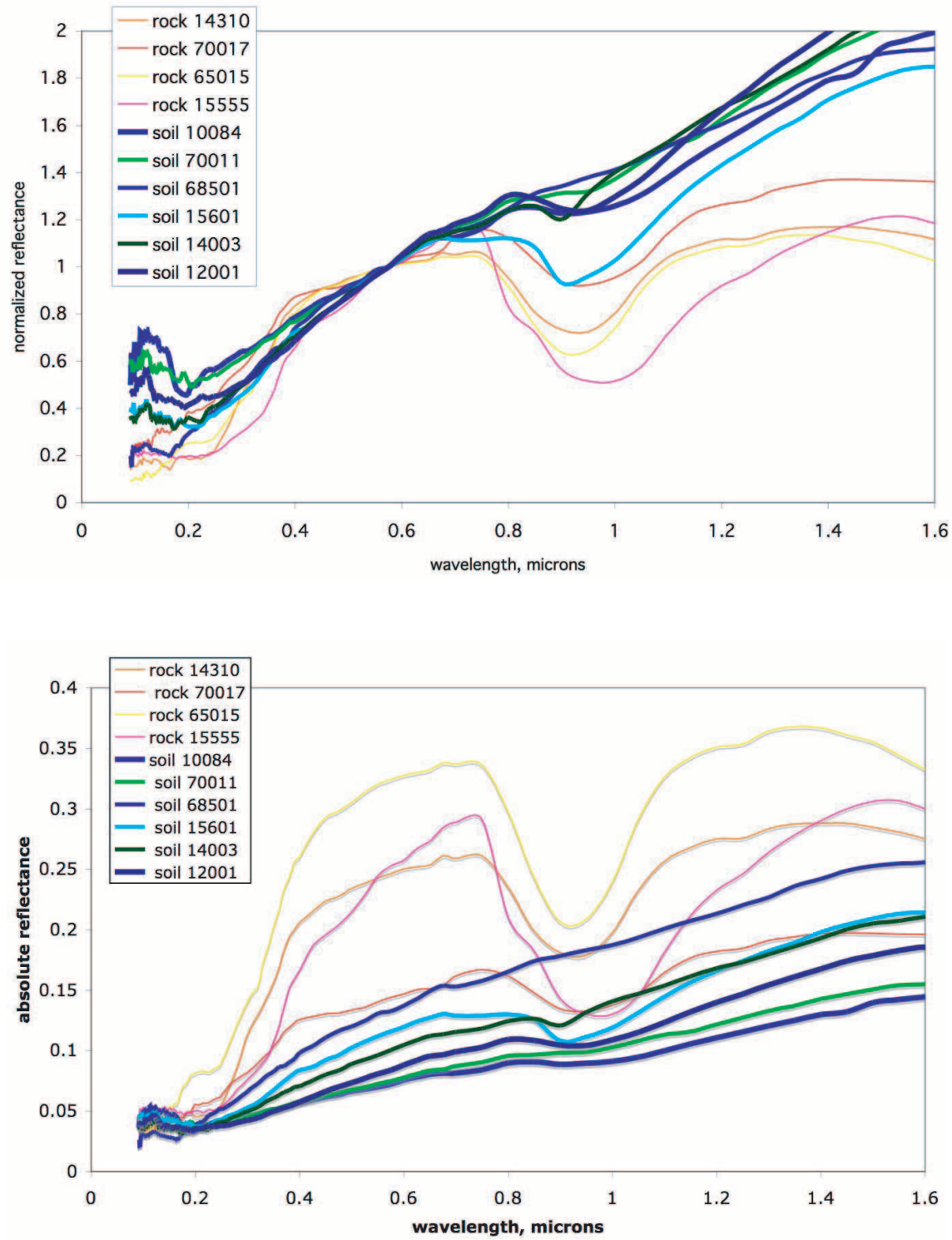

FIG. 1.—Laboratory spectra of lunar soils (*thick lines*) and powdered rocks (*thin lines*) (from Wagner et al. 1987). *Top*: Spectra scaled to unity at 0.35 μm to enhance variations in slopes. *Bottom*: Spectra plotted on an absolute scale to display relative brightness variations. The more weathered lunar soils are redder in the VNIR but bluer in the UV region shortward of ~0.4 μm compared to the less weathered powdered lunar rock samples.

UV data of asteroid 4 Vesta, and laboratory space weathering experiments.

2.1. *The Moon and Lunar Samples*

Apollo 17 UV spectrograph measurements first displayed the lunar spectral reversal, where it was noted that the visibly dark lunar maria are 5%–10% brighter than the highlands at far-UV (FUV) wavelengths (147 nm; Lucke et al. 1974); the phenomenon was confirmed in *Extreme Ultraviolet Explorer* images (Flynn et al. 1998). The lunar spectral reversal was linked to space weathering when it was found that lunar soils, which have been exposed to more weathering, exhibit the spectral reversal, while powdered lunar rocks do not (Wagner et al. 1987). The

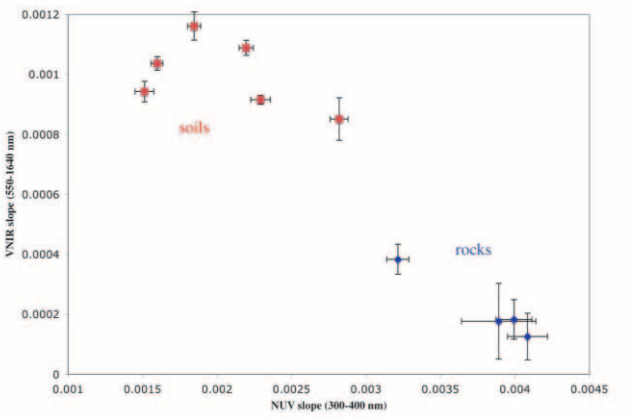

FIG. 2.—Spectral slopes (in units of reflectance nm^{-1}) of lunar samples, showing trends with weathering. Error bars represent the 1 σ uncertainty on the computed slopes. Lunar soils are redder at VNIR wavelengths and bluer in the UV than lunar rocks.

lunar spectral reversal is due in part to the higher index of refraction of mare material relative to highlands material (Henry et al. 1976). At shorter wavelengths, surface scattering dominates over volume scattering so that reflectance is directly related to the index of refraction (Henry et al. 1976). The index of refraction of many materials increases with decreasing wavelength, so that they become brighter at shorter wavelengths. However, the correlation between visibly bright and UV-dark lunar regions as seen by *Apollo 17* is imperfect, and UV spectra may therefore contain more information than what is known from visible spectra (Henry et al. 1976). In particular, since FUV radiation is less penetrating than visible radiation, short wavelengths are more sensitive to thin coatings on grains that may be the result of weathering processes (Lucke et al. 1974).

Laboratory spectra of lunar samples in the UV–IR wavelength ranges (from Wagner et al. 1987) are shown in Figure 1. Longward of ~0.6 μm, lunar soils are clearly redder (and darker) than crushed lunar rocks. At UV wavelengths, the opposite is true: in this range, lunar rocks are spectrally redder than lunar soils. We have investigated these lunar samples over the entire UV wavelength range and found that the strongest difference between the soils and rocks occurs in the 0.3–0.4 μm range, where the lunar rocks display a steep UV drop-off that is greatly reduced in the lunar soils. In addition, shortward of 0.2 μm the lunar soils' spectra tend to display an upturn in brightness, which corresponds to the spectral reversal. In Figure 2 we plot the spectral slopes of the lunar rocks and soils at near-UV (NUV) (300–400 nm) and VNIR (550–1640 nm) wavelengths, where the slopes have been computed by fitting a straight line to the reflectance data in each wavelength range. The trend is obvious: the less weathered crushed lunar rocks generally have lower (less red) VNIR slopes and higher (redder) UV slopes, while the more weathered lunar soils generally have higher (redder) VNIR slopes and lower (bluer) UV slopes.

2.2. *Vesta*

Vesta, a V-class asteroid made up largely of mafic silicates, does not exhibit strong indications of space weathering at VNIR wavelengths. Vesta is a large asteroid, whose pyroxene-rich surface is mostly spectrally similar to Howardite-Eucrite-Diogenite (HED) meteorites, suggesting that, although old, its surface does not exhibit lunar-like space weathering at VNIR wavelengths. However, analysis of *International Ultraviolet Explorer* (*IUE*) spectra of Vesta (Hendrix et al. 2003) shows that UV spectra of Vesta display evidence of lunar-like UV space weathering on a global scale (compared with meteorite spectra), as well as in relative amounts across the surface. At UV–visible wavelengths, Vesta is spectrally bluer than HED meteorites (meteorites potentially derived from Vesta), particularly diogenite and eucrite samples (Hiroi et al. 1994; Hendrix et al. 2003). Because it is known that Vesta's VNIR spectra do not display strong lunar-like space weathering characteristics, these results suggest that Vesta has undergone enough weathering to affect the blue part of the spectrum moderately but not enough to strongly alter the VNIR spectrum. Another possibility is that weathering effects for V-type asteroids are somewhat different than for the Moon (and S-type asteroids); the weathering effects appear only at UV–visible wavelengths and not at VNIR wavelengths.

IUE data of Vesta (Hendrix et al. 2003) covering more than one rotation period indicate that Vesta's UV light curve is offset by almost 180° from the visible light curve, indicating that this asteroid displays a spectral reversal. Regions on Vesta's surface that are relatively bright in the visible are relatively dark at near-UV wavelengths (particularly longward of ~290 nm). This suggests that Vesta's surface may have undergone varying amounts of space weathering. A global comparison between Vesta's topographic map and its *IUE*-derived light curve (Hendrix et al. 2003) suggests that the UV-dark region corresponds to the "fresher" overturned material related to the south pole crater. Correspondingly, the UV-bright western hemisphere is dominated by a large region of average height, suggesting that this region has not been affected by major impact or accumulation of material after impact. This western region is thus likely to be older than the exposed topographically low and high places, and may have thus experienced more extensive weathering effects. Vesta's spectral reversal, and the relative UV brightness of the older western hemisphere, may be due to the longer exposure time of this region to space, allowing it to have accumulated more SMFe (Hapke 2001). The spectral reversal could also be due to hemispherical compositional variations combined with the weathering process.

2.3. *Experimental Laboratory Data and Models*

Laboratory experiments studying the effects of space weathering on minerals, meteorite samples, and lunar samples (e.g., Clark et al. 1992; Moroz et al. 1996; Hiroi & Pieters 1998; Hapke 2001) have focused on the VNIR wavelength region, in attempts to mimic the weathering effects seen in that wavelength range. Visual inspection of the spectra produced by those researchers demonstrates that the UV–visible wavelength region exhibits dramatic changes in response to simulated weathering processes.

Clark et al. (1992) displayed spectra of ordinary chondrite meteorites (H6 Ozona, L6 Lacriolla, and H5 Nuevo Mercurio), both unaltered and after a process involving melting, recrystallization, and comminution of the samples in an attempt to simulate weathering on asteroids. Clark et al. described the effects of the simulated weathering as a decrease in reflectance, a decrease in absorption band depth (referring to the 0.95 μm band), and an increase in the slope of the continuum. Inspection of Clark et al.'s figures reveals that the altered samples have a much bluer slope shortward of ~0.55 μm compared with the altered samples. This is seen in all three meteorites for all grain sizes.

Moroz et al. (1996) performed space-weathering simulation experiments on meteorite and mineral samples by impulse laser treatment. At VNIR wavelengths, altered samples showed an increase in spectral slope and a decrease in band depth along with an overall darkening of the spectrum. Along with these

TABLE 1
S-TYPE ASTEROIDS

Object	Taxonomic Type[a]	Visible Albedo	Radius (km)	Observation Date	Phase Angle (deg)	Observation Name
3 Juno	S(IV), Sk	0.2383	123	1979 Sep 24	29.5	LWR05678LL, LWR05679LL
6 Hebe	S(IV), S	0.2679	92.6	1980 Dec 13–14	19	LWR09488LL, LWR09495LL, LWR09496LL
7 Iris	S(IV), S	0.2766	99.9	1980 Dec 13	31.7	LWR09487LL
8 Flora	S(III)	0.2426	67.9	1980 May 30	3.1	LWR07901LL, LWR07902LL
9 Metis	S(I)	0.13	95	1981 Jun 17–18	6.7, 7.1	LWR10880LL, LWR10893LL
14 Irene	S, S	0.16	76.5	1980 May 28, 30	9.41, 10	LWR07883LL LWR07900LL
15 Eunomia	S(III), S	0.2094	127.7	1980 May 30	13.9	LWR07903LL
18 Melpomene	S(V), S	0.2225	70.3	1984 Jun 28–29	13.8, 14.1	LWP03671LL, LWP03675LL
20 Massalia	S(VI), S	0.2096	72.8	1981 May 13–14	25.2	LWR10598LL, LWR10612LL
23 Thalia	S, S	0.2536	53.8	1980 Dec 15	4.5	LWR09499LL, LWR09500LL
27 Euterpe	S(IV), S	0.16	58.5	1979 Dec 28	8.5	LWR06484LL
29 Amphitrite	S(V), S	0.1793	106.1	1981 Jun 15–16	11.2, 11.6	LWR10865LL, LWR10866LL, LWR10873LL
40 Harmonia	S(VII), S	0.2418	53.8	1982 Jan 6	20.3	LWR12297LL
42 Isis	S(I), L	0.1712	50.1	1982 Jul 22	17.6	LWR13751LL
63 Ausonia	S(II, III), Sa	0.1586	51.6	1980 May 28, 30	17.6, 18.3	LWR07879LL, LWR07880LL, LWR07899LL
89 Julia	S, K	0.1764	75.7	1982 Jan 8	6.9	LWR12305LL
182 Elsa	S, S	0.2083	21.8	1993 Nov 4	17.1	Y19Y0402
243 Ida	S, S	0.2382	58×23	1993 Aug 28	25	...
354 Eleonora	S(I), Sl	0.1948	77.6	1982 Jan 7	13.2	LWR12298LL
433 Eros	S(IV), S	0.25	17.5×6.5	1982 Jan 7	48.8	LWR12302LL
471 Papagena	S, S	0.1994	69.5	1982 Jan 8	12.1	LWR12304LL
532 Herculina	S(III), S	0.1697	111.1	1982 Jan 7	10.5	LWR12300LL
951 Gaspra	S, S	0.19	17×10	1991 Oct 29	39	...
1620 Geographos	S, S	0.3258	$5 \times 2 \times 1.5$	1994 Aug 26	41, 42, 42.7	LWP29003LL, LWP29004LL, LWP29005LL

[a] Taxonomic types from Tholen (1989), Gaffey et al. (1993), and Bus & Binzel (2002).

effects, ordinary chondrite Elenovka L5, carbonaceous chondrite Allende CV3, and an olivine sample also revealed a spectral bluing at the shorter wavelengths ($\lesssim 0.55$ μm); such a trend is possibly also apparent in the clinopyroxene sample and the olivine-clinopyroxene mixture as well.

Hiroi & Pieters (1998) showed spectra of the Johnstown diogenite before and after laser irradiation. The irradiated sample is darker at all wavelengths and redder at wavelengths $\gtrsim 0.6$ μm, and appears to be somewhat spectrally bluer at wavelengths $\lesssim 0.5$ μm. Similarly, Brunetto & Strazzulla (2005) (and Strazzulla et al. 2005) performed irradiation experiments to simulate weathering of asteroids by solar-wind ions. Their silicate samples are redder and darker at VNIR wavelengths after irradiation, and the UV–visible region is distinctly bluer (shortward of ~ 0.5 μm).

Hapke (2001; originally in Hapke 1977) displayed spectra of lunar sample 10022, a pulverized lunar rock, before and after irradiation by 2 keV H ions. The irradiated sample is darker overall than the unirradiated sample, at all wavelengths. The primary change in slope is seen at wavelengths $\lesssim 0.4$ μm, where the unirradiated sample has a steep slope and the slope of the irradiated sample is relatively flat.

A light-scattering model (Hapke 2001) in which a silicate powder is modeled with the addition of increasing amounts of nanophase iron to simulate space-weathering effects, shows that the UV–visible wavelength region is dramatically affected after the addition of very small amounts of nanophase iron. With the addition of just 0.1% SMFe, the entire spectrum decreases in brightness, with a particularly sharp decrease in brightness at wavelengths $\lesssim 0.5$ μm. With the addition of 0.5% SMFe, the slope shortward of ~ 0.5 μm begins to become bluer, and with the addition of 2% SMFe, the slope shortward of ~ 0.5 μm flattens out. The spectral behavior is attributed to the absorbing nature of iron at the shorter wavelengths (Hapke 2001). With the addition of more nanophase iron, the UV–visible part of the spectrum flattens out. This reflectance modeling suggests that the UV–visible wavelength region is particularly sensitive to added amounts of SMFe and is in fact more sensitive to the addition of small amounts of SMFe than longer wavelengths.

3. NEW WORK: S-TYPE ASTEROIDS

To further investigate the idea that weathered surfaces are bluer at NUV wavelengths, we study the existing set of UV observations of S-type asteroids from *IUE*, the *Hubble Space Telescope* (*HST*), and *Galileo*. We compare the UV spectral slopes of the asteroids with the spectral slopes of ordinary chondrite meteorites (presumably derived from S-class asteroids) measured in the laboratory (Wagner et al. 1987). We compare UV asteroid-meteorite comparisons with VNIR asteroid-meteorite trends by using asteroid spectra from ground-based telescopes.

3.1. *Data Sets and Reduction*

The observations used in this analysis are listed in Table 1. This list represents all of the NUV spectra of S-class asteroids that are publicly available. The *IUE* data used in this study were obtained from the INES (*IUE* Newly Extracted Spectra) Web site.[2] The NEWSIPS versions of these spectra have been published elsewhere (Roettger & Buratti 1994). The INES files benefit from an improved geometric correction, a more accurate photometric correction, and an increased signal-to-noise ratio of the extracted *IUE* data through the use of new processing algorithms (Wamsteker & Gonzelez-Riestra 1998). Spectra were taken with the Long Wavelength Prime and Redundant (LWP and LWR) spectrographs, which cover the 185–335 nm wavelength range with a spectral spacing of 0.27 nm. The *IUE* data

[2] Available at http://ines.laeff.esa.es.

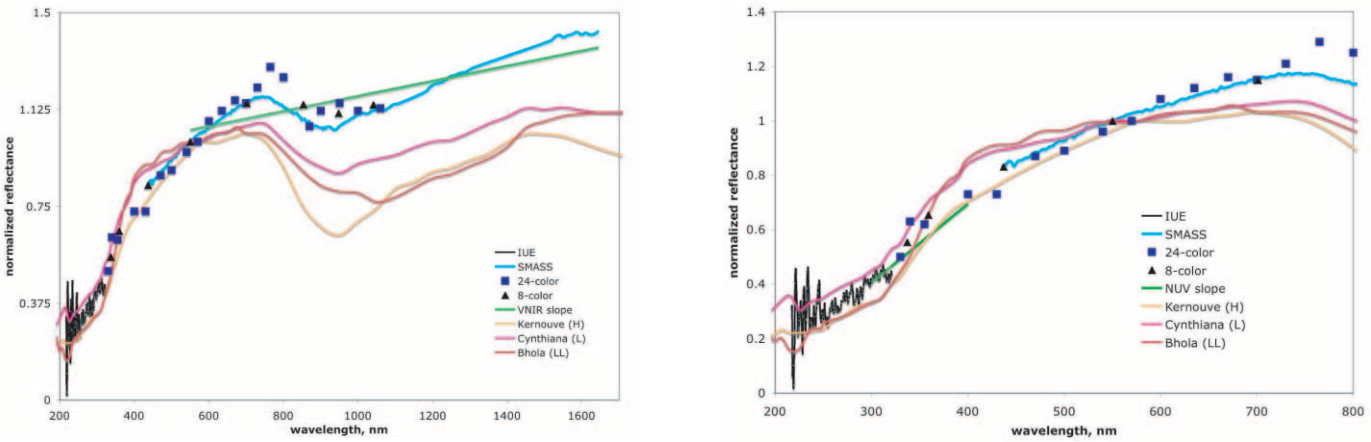

FIG. 3.—Composite reflectance spectrum of a sample S-class asteroid, 7 Iris, over the UV–NIR range (*left*) and over the UV–visible wavelength range (*right*). The *IUE* data cover the ~220–~320 nm range, while ground-based data cover the ~320–1650 nm range. Overplotted are sample laboratory spectra of ordinary chondrite meteorites. Straight-line fits for NUV and VNIR slopes are shown in green. The comparison between S-class asteroids and OC meteorites is similar to the comparison between lunar soil samples and lunar rock samples (Fig. 1); asteroid data do not exist at shorter UV wavelengths, so it is unclear whether S-class asteroid spectra display the upturn in brightness seen in the lunar soils shortward of 0.2 μm.

set is supplemented with one *HST* spectrum of an S-class asteroid (182 Elsa) and *Galileo* Ultraviolet Spectrometer (UVS) spectra of 243 Ida and 951 Gaspra. The Faint Object Spectrograph (FOS) observation covers the 222–326 nm wavelength range with a spectral spacing of 0.05 nm. The Galileo observations used in this study were taken using the UVS *F* channel (162–323 nm, with a 0.32 nm spectral element spacing). These spectra have been previously analyzed (Hendrix 1996).

To determine the reflectance measured in the *IUE* and *HST* observations, we converted the spectra to photons $cm^{-2}\ s^{-1}\ Å^{-1}$ for division by the solar spectrum. For all observations we used a solar spectrum from UARS SOLSTICE (Rottman et al. 1993), corrected to an Earth-Sun distance of 1.0 AU. The observations were corrected for satellite-Sun and satellite-Earth distances at the time of each measurement. Thus, the equation that was used to determine spectral reflectance for each *IUE* and *HST* measurement was

$$\mathrm{ref}(\lambda) = D(\lambda)\,\lambda K \frac{\Delta^2}{F(\lambda)}\Omega, \qquad (1)$$

where the variables are as follows:

$D(\lambda)$.—Raw data, in ergs $cm^2\ s^{-1}\ Å^{-1}$.
K.—Conversion factor from ergs to photons, 5.028×10^7.
Ω.—(Satellite radius/δ)^2 (each in kilometers).
$F(\lambda)$.—Solar spectrum, in photons $cm^{-2}\ s^{-1}\ Å^{-1}$.
Δ.—Distance between satellite and Sun, in AU.
δ.—Distance between satellite and Earth.

For each *Galileo* UVS observation, the background signal was subtracted, then the calibration curve applied; the resulting measured spectral intensity was then divided by the solar spectrum. Generally the background signal is due to radiation background and is approximated by averaging the first ~100 spectral elements, or the signal shortward of ~200 nm, where no reflected sunlight is measured. In determining the reflectance the filling factor was accounted for, since these disk-integrated observations were performed at distances such that the $0\overset{\circ}{.}1 \times 0\overset{\circ}{.}4$ *F*-channel field of view was not filled.

The asteroid UV reflectance spectra were combined with ground-based spectra of the same bodies at VNIR wavelengths to create composite spectra spanning a large wavelength range. The VNIR data were pulled from the 24 color database (Chapman & Gaffey 1979; McFadden et al. 1984), the Small Main-Belt Asteroid Spectroscopic Survey (SMASS) database (Xu et al. 1995; Burbine & Binzel 2002; Bus & Binzel 2002), the 8 color database (Zellner et al. 1985), the 7 color database (Clark et al. 1995), and the 52 color database (Bell et al. 1984, 1988). The Eros spectrum was supplemented with data from Vilas & McFadden (1992). The VNIR reflectance spectra were converted to absolute reflectance spectra by scaling by the visible geometric albedo (0° phase) (*Infrared Astronomical Satellite*, Tedesco et al. 2002; 9 Metis albedo, Lagerros et al. 1999; 433 Eros albedo, Clark et al. 2002b). The UV data from *IUE*, *Galileo*, and *HST* usually overlap slightly or nearly overlap with 24 color data or 8 color data; these UV spectra, from phase angles larger than 0°, are scaled to align with the longer wavelength data in the overlapping wavelength region. We assume here that phase angle differences do not affect the spectral slope in the UV, a reasonable assumption given the relatively small wavelength range under study. The only publicly available long-wavelength data for 182 Elsa are the seven color data covering 0.9–2.3 μm. The gap in data between the *HST* spectrum (0.23–0.33 μm) and the seven color data is large enough that it is difficult to extrapolate slopes in the intervening visible region, so we do not include that asteroid in this analysis. The composite spectra of the S-class asteroids were compared with the laboratory data of ordinary chondrite meteorites as measured by Wagner et al. (1987). The meteorite laboratory spectra span the 0.1–2 μm range. Figure 3 shows a sample composite asteroid spectrum in the UV–VNIR wavelength range, with ordinary chondrite (H, L, LL) spectra overplotted.

The spectral slope of each asteroid composite spectrum was measured in various wavelength ranges by obtaining straight-line fits. The VNIR slope was obtained by obtaining a straight-line fit to the data in that range, usually SMASS data. The SMASS data for 8 Flora and 1620 Geographos only extend to ~900 nm, so the VNIR slope was obtained by fitting to seven color data. For 433 Eros and 532 Herculina, SMASS data only exist out to ~900 nm and seven color data do not exist, so the composite spectra were supplemented with data from Murchie & Pieters (1996) for Eros and 52 color data for Herculina. No long-wavelength data of asteroid 23 Thalia and 471 Papagena are publicly available.

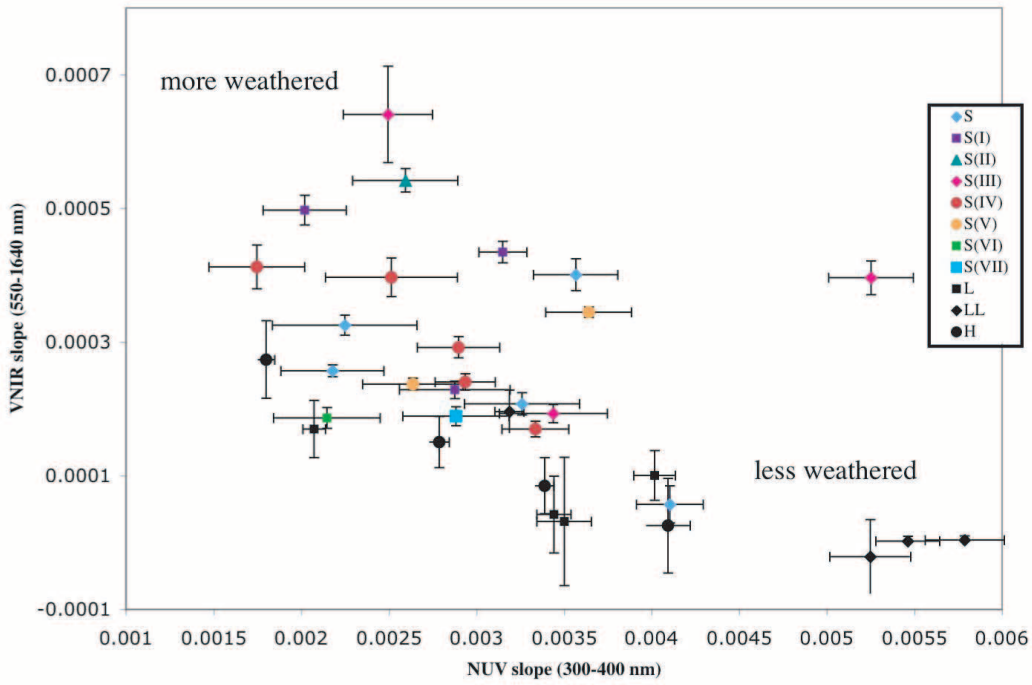

FIG. 4.—Spectral slopes (in units of reflectance nm^{-1}) of S-class asteroids and ordinary chondrites. Error bars represent the 1 σ uncertainty on the computed slopes. S-class asteroids are generally redder at VNIR wavelengths and bluer in the UV than ordinary chondrite meteorites.

Where discrepancies exist between the 8 color data and the 24 color data, we used the 24 color data in obtaining the NUV slope.

3.2. *Results: NUV-VNIR Slope-Slope Plot*

In order to look for trends, the spectral slopes of the asteroids and meteorites were measured in various wavelength ranges. Spectral slopes were determined for the 200–250, 250–300, 200–300, 350–500, 300–400, and 250–400 nm ranges. We find that the strongest trend is seen in the 300–400 nm range compared with VNIR wavelengths. Figure 4 is a slope-slope plot displaying the asteroid and meteorite slopes measured in the 300–400 nm (NUV) range versus the slopes measured in the 550–1640 nm (VNIR) range. The measured NUV slopes of the S-class asteroids studied here are lower (bluer) than the slopes of most of the OC meteorites in the Wagner et al. (1987) database. Correspondingly (as previously known), the VNIR slopes of the S-type asteroids are higher (redder) than those of the OC meteorites. In other words, the comparison between S asteroids and OC meteorites is similar to the comparison between lunar soils and lunar rocks (Fig. 2). Table 2 displays the measured slopes for each object as shown in Figure 4.

The results shown in Figure 4 suggest that there is a variation among the sampled asteroids in exposure ages. For instance, 3 Juno, 15 Eunomia, and 1620 Geographos fall into a region on Figure 4 of fresher, less weathered surfaces, compared to 8 Flora, 63 Ausonia, 354 Eleonora, and 433 Eros, which may be older surfaces based on these results.

Asteroid 3 Juno exhibits spectral variations across the surface that have been linked to a possible large, relatively fresh impact feature (Baliunas et al. 2003). This complicates our analysis because we use the NUV slope averaged from several *IUE* observations. It is possible that the large fresh region on Juno was observed by *IUE* and dominates the NUV slope. We plan to investigate UV spectral variations with Juno latitude and longitude in a future study. Asteroid 15 Eunomia has been postulated to be the parent body of the Eunomia family. Recent observations of 15 Eunomia (Nathues et al. 2005) suggest that the outer layer of Eunomia has been stripped off, likely during the impact that created the Eunomia family. This may suggest that the current surface of Eunomia is relatively young, which may explain its relatively red NUV spectral slope. Geographos, a near-Earth asteroid, has a very red NUV slope along with a very blue VNIR slope, suggesting a young, unweathered surface.

Asteroid 433 Eros may have a very weathered surface based on this NUV analysis, consistent with previous work. As discussed by Clark et al. (2002b), albedo contrasts and associated spectral variations on Eros are most consistent with a combination of enhanced dark spectrally neutral components and lunar-like optical maturation. Izenberg et al. (2003) point out that Eros exhibits a brightness variation consistent with lunar-like space weathering but not significant spectral variation; they contrast this type of weathering with Ida-like space weathering in which spectral variation is exhibited without strong brightness variations. Such a variation of weathering effects suggests that the weathering effects are dependent on surface composition. Asteroid 8 Flora has a moderately blue UV slope along with an extremely red VNIR slope, suggesting that it is quite weathered. The VNIR spectrum of Flora has been previously discussed by Gaffey (1984), who also found a large discrepancy between the spectrum of Flora and OC meteorites. Rotationally resolved VNIR spectra of 354 Eleonora (Mothe-Diniz et al. 2000) show little spectral variation with rotation of the asteroid. This could suggest that no recent impact has exposed large amounts of fresh material on the surface and that the surface is uniformly aged and weathered. However, we note that Mothe-Diniz et al. (2000) interpreted the lack of rotational variability, along with the classification by Gaffey et al. (1993) of 354 Eleonora as a transitional A/S object due to

TABLE 2
NUV and VNIR Slopes: S Asteroids and OC Meteorites

Object	VNIR Slope	NUV Slope
3	0.000170058	0.00333530
6	0.000240285	0.00293552
7	0.000292070	0.00289734
8	0.000640628	0.00249387
9	0.000434595	0.00315015
14	0.000257102	0.00217817
15	0.000192905	0.00343817
18	0.000344729	0.00364002
20	0.000186520	0.00214573
23	...	0.00308889
27	0.000396841	0.00251409
29	0.000237191	0.00263601
40	0.000189097	0.00288241
42	0.000228627	0.00287592
63	0.000542073	0.00259347
89	0.000400679	0.00356579
243	0.000325359	0.00224744
354	0.000497581	0.00201924
433	0.000412566	0.00174654
471	...	0.00208717
532	0.000396117	0.00525249
951	0.000207704	0.00325924
1620	5.72514E−05	0.00410346
Cynthiana (L)	0.000100388	0.00401552
Hallingeberg (L)	0.000169693	0.00207347
Malakal (L)	4.19156E−05	0.00344147
Tathlith (L)	3.15680E−05	0.00350033
Bandong (LL)	−2.09897E−05	0.00524815
Bhola (LL)	3.59182E−06	0.00578691
Chainpur (LL)	0.000196068	0.00318761
Khanpur (LL)	2.39213E−06	0.00546229
Ankober (H)	0.000273877	0.00179931
Bremervorde (H)	0.000150337	0.00278627
Forest City (H)	8.51221E−05	0.00338779
Kernouve (H)	2.52128E−05	0.00409320

Note.—VNIR slope = 550–1640 nm nm^{-1}. NUV slope = 300–400 nm nm^{-1}.

its olivine content, as being due to a recent large impact that stripped away the entire outer surface.

Asteroid 532 Herculina is a standout on our slope-slope plot. Herculina's NUV slope is extremely red, while its VNIR slope is also quite red. Taylor et al. (1987) note that Herculina has an interesting light curve, suggesting spatial variations in brightness across the surface. The UV data also suggest that this asteroid would make a very interesting target for future observations.

3.2.1. *Correlation with S-Type Subclasses*

Figure 4 identifies the taxonomic subclasses of the asteroids in this database (when they exist), based on Tholen (1989) and Gaffey et al. (1993). (Table 1 also lists the subclasses as defined by Bus & Binzel [2002], but our data set includes so few asteroids in that taxonomy that we cannot look for correlations here.) Within this data set the largest number of any subclass is five of the pyroxene-rich S(IV) types. Although it is a small sample, there does appear to be a good correlation between NUV slope and VNIR slope (linear regression correlation coefficient = 81%). Gaffey et al. (1993) found that within the S(IV) subclass there is a strong trend toward reduced VNIR spectral slope with increasing diameter, suggesting that red slope is anticorrelated with surface age in this subclass, contrary to expectations. Such a trend appears to be consistent with the NUV results presented here; however, it is likely premature to draw conclusions based on such a small sample of S(IV) asteroids. We note that Juno, the largest S(IV) asteroid, also has the reddest NUV slope (and bluest VNIR) slope, contrary to expectations, but as previously discussed, spectral characteristics on that asteroid could be due to relatively fresh regions across the surface. For the entire UV S-class data set, we do not find a strong trend between S-asteroid size and NUV slope.

4. DISCUSSION

As previously discussed, the source of asteroid weathering effects is not fully understood: B. Hapke (Hapke et al. 1975; Hapke 2001) has proposed that the formation of nanophase iron particles in coatings on regolith grains as a result of micrometeoroid impacts or irradiation by the solar wind is the main cause of the change in the VNIR spectral properties on the Moon and S-type asteroids. Such nanophase iron particles have been detected after pulse laser irradiation experiments within the amorphous vapor-deposited rims of olivine grains (Keller et al. 2000; Sasaki et al. 2001). Other researchers (e.g., Marchi et al. 2005; Strazzulla et al. 2005) contend that heavy ion bombardment is the source of weathering effects in asteroids, particularly in the near-Earth environment (Brunetto & Strazzulla 2005; Marchi et al. 2006).

The results presented here may be most consistent with the addition of nanophase iron. For S-class asteroid spectra across the UV-NIR wavelength region, these results show that a trend in spectral slope is seen in the 300–400 nm range. The slope in this range is significantly bluer for S-class asteroids than for OC meteorites. This is the same trend that is seen in lunar samples, for which lunar soils are bluer in the 300–400 nm range than lunar rocks. An explanation for the bluing is that the UV absorption edge, which is present in nearly all silicates, is degraded in the weathered surfaces. This is analogous to the diminished absorption features seen in weathered surfaces at NIR wavelengths.

Such an effect is consistent with the presence, in the weathered bodies, of additional iron or iron-bearing minerals. Opaque materials (such as iron) are dominated by surface scattering, which is controlled by Fresnel reflection (Wagner et al. 1987) and are thus spectrally flat over a wide range of wavelengths; in opaques, there is no absorption edge in the 150–450 nm region (Fig. 5). In contrast, nonopaque materials are dominated by volume scattering at VNIR wavelengths, at which the intensity of the reflected light is inversely proportional to wavelength. In nonopaque materials, the transition to surface scattering occurs in the 150–450 nm region (Wagner et al. 1987) and is marked by a minimum in reflectance. Thus, compared to materials such as pyroxenes and feldspars, iron-bearing minerals can be relatively bright at FUV-NUV wavelengths. In the 150–450 nm range, iron-bearing minerals also differ from nonopaque materials in spectral shape, where the nonopaque materials experience a decrease in brightness as they transition from reflectance dominated by volume scattering to reflectance dominated by surface scattering, and opaque materials tend to be spectrally flat. As a result, we expect surfaces consisting of iron-bearing minerals to be less spectrally red in the 150–450 nm range and possibly even brighter than surfaces with lower amounts of iron-bearing minerals.

The results presented here suggest that the UV absorption edge is "weathered away" in asteroids and lunar soils (as is the 0.9 μm band), possibly due to the addition of nanophase iron to grain coatings, making the NUV spectral slope blue compared to unweathered materials of similar composition. The difference between the disappearance of the 0.9 μm band and the UV absorption edge is that the loss of the UV band seems to occur with the addition of lower amounts of SMFe, as previously discussed. With the addition of larger amounts of nanophase iron, the 0.9 μm

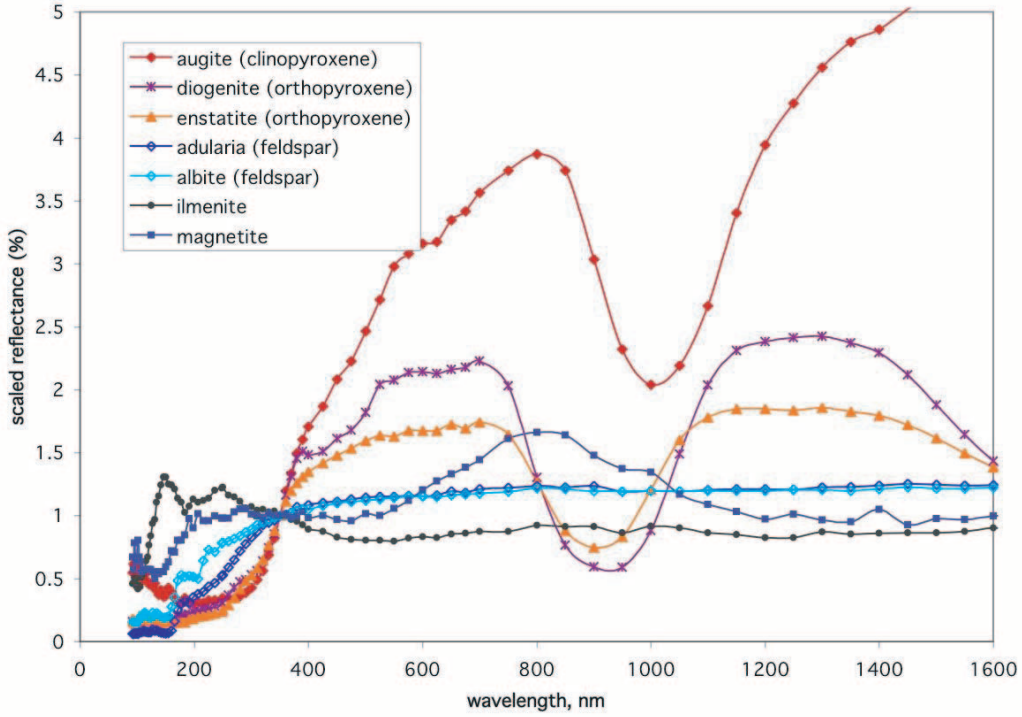

FIG. 5.—Reflectance spectra of lunar-like minerals at UV–NIR wavelengths. Pyroxenes, feldspars, and olivines all exhibit a UV drop-off in the 150–450 nm range that is not seen in iron-bearing minerals (e.g., ilmenite and magnetite).

band begins to disappear. The change in spectral slope that is a result of a decrease in the UV drop-off possibly due to weathering-derived nanophase iron suggests that surfaces of different materials will manifest weathering in different ways. For example, a surface with a high feldspar or orthopyroxene content (usually having a steep UV drop-off) could exhibit weathering effects at UV wavelengths with lower amounts of weathering than an asteroid primarily composed of clinopyroxene or olivine (generally not as steep of a UV drop-off).

These effects are also related to grain size. The intensity of volume-scattered light goes as $\sim \exp(-\alpha D)$, where $\alpha = 4\pi k/\lambda$ and D is the grain diameter. The intensity of surface scattering is proportional to the Fresnel reflection coefficient: $R \sim [(n-1)^2 + k^2]/[(n+1)^2 + k^2]$. Surface scattering is thus dependent only on the optical constants (n, k) of the material and is independent of grain size. At VNIR wavelengths, space-weathering effects are detected primarily in fine regoliths (e.g., Pieters et al. 1993), in which the particles are small enough that the fine-grained metal opaques have an increased contribution. Shorter wavelengths are more sensitive to coatings on particles, whether the grains are small or large. A possible scenario is that a young surface with small amounts of weathering will have some amount of nanophase iron present in a regolith composed of larger grains; the result is a bluing of the UV spectrum as the UV absorption band diminishes. With more weathering, the grains in the regolith become finer, and more nanophase iron is added; at this point, the typical lunar-like space-weathering effects are also seen in VNIR spectra.

5. SUMMARY

Composite spectra (200–1600 nm) of S-class asteroids have been created by combining *IUE* spectra with ground-based data and compared with laboratory spectra of ordinary chondrites over the same spectral range. The VNIR slopes (550–1640 nm) are well correlated with the NUV (300–400 nm) slopes, and the correlation suggests that surfaces that are spectrally redder in the VNIR are also spectrally bluer in the NUV. The relative blue spectral slope in the NUV can be explained by a decrease in the strength of the UV absorption feature that appears in most lunar-like and asteroid-like minerals as a result of a transition between volume scattering and surface scattering; minerals with high iron content do not exhibit the UV drop-off. The addition of nanophase iron to the coatings of weathered grains results in the decrease in the NUV slope of these weathered surfaces. The "typical" effects of darkening and decrease in absorption band strength that characterize weathering at VNIR wavelengths also apply at NUV wavelengths; however, instead of a spectral reddening with weathering, there is a spectral bluing. The NUV spectral bluing likely occurs with a lower amount of weathering than the reddening at VNIR wavelengths. Lunar weathering effects also appear to include an upturn in reflectance at wavelengths shorter than 200 nm. Whether S-class asteroids also display an upturn in reflectance at short UV wavelengths remains to be seen; good-quality spectra of asteroids at those wavelengths do not exist.

We are grateful to Jeff Wagner for providing laboratory data of lunar samples and meteorites. Simone Marchi supplied very helpful comments and suggestions on the manuscript. Support for program AR10319 was provided by NASA through a grant from the Space Telescope Science Institute, which is operated by the Association of Universities for Research in Astronomy, Inc., under NASA contract NAS5-26555. This work was performed at the Jet Propulsion Laboratory, California Institute of Technology, under contract with the National Aeronautics and Space Administration.

REFERENCES

Baliunas, S., Donahue, R., Rampino, M. R., Gaffey, M. J., Shelton, J. C., & Mohanty, S. 2003, Icarus, 163, 135
Bell, J. F., Hawke, B. R., Gaffey, M. J., & Owensby, P. D. 1984, BAAS, 16, 692
Bell, J. F., Hawke, B. R., Owensby, P. D., & Gaffey, M. J. 1988, Lunar Planet. Sci. Conf., 19, 57
Binzel, R. P., Rivkin, A. S., Stuart, J. S., Harris, A. W., Bus, S. J., & Burbine, T. H. 2004, Icarus, 170, 259
Brunetto, R., & Strazzulla, G. 2005, Icarus, 179, 265
Burbine, T. H., & Binzel, R. P. 2002, Icarus, 159, 468
Bus, S. J., & Binzel, R. P. 2002, Icarus, 158, 146
Chapman, C. R. 1996, Meteoritics Planet. Sci., 31, 699
Chapman, C. R., & Gaffey, M. J. 1979, in Asteroids, ed. T. Gehrels (Tucson: Univ. Arizona Press), 1064
Clark, B. E., Bell, J. F., Fanale, F. P., & O'Connor, D. J. 1995, Icarus, 113, 387
Clark, B. E., Fanale, F. P., & Salisbury, J. W. 1992, Icarus, 97, 288
Clark, B. E., Hapke, B., Pieters, C., & Britt, D. 2002a, in Asteroids III, ed. W. F. Bottke et al. (Tucson: Univ. Arizona Press), 585
Clark, B. E., et al. 2002b, Icarus, 155, 189
Flynn, B. C., Vallerga, J. V., Gladstone, G. R., & Edelstein, J. 1998, Geophys. Res. Lett., 25, 3253
Gaffey, M. J. 1984, Icarus, 60, 83
Gaffey, M. J., Bell, J. F., Brown, R. H., Burbine, T. H., Piatek, J. L., Reed, K. L., & Chaky, D. A. 1993, Icarus, 106, 573
Hapke, B. 1977, Phys. Earth Planet. Inter., 15, 264
———. 2001, J. Geophys. Res., 106, 10039
Hapke, B., Cassidy, W., & Wells, E. 1975, Moon, 13, 339
Helfenstein, P., et al. 1994, Icarus, 107, 37
Hendrix, A. R. 1996, Ph.D. thesis, Univ. Colorado
Hendrix, A. R., Vilas, F., & Festou, M. C. 2003, Icarus, 162, 1
Henry, R. C., Fastie, W. G., Lucke, R. L., & Hapke, B. W. 1976, Moon, 15, 51
Hiroi, T., & Pieters, C. M. 1998, in Antarctic Meteorite Research, ed. T. Hirasawa (Tokyo: Natl. Inst. Polar Research), 163
Hiroi, T., Pieters, C. M., & Takeda, T. 1994, Meteoritics, 29, 394
Izenberg, N. R., Murchie, S. L., Bell, J. F., III, McFadden, L. A., Wellnitz, D. D., Clark, B. E., & Gaffey, M. J. 2003, Meteoritics Planet. Sci., 38, 1053
Jedicke, R., Nesvorny, D., Whiteley, R., Ivezic, A., & Juric, M. 2004, Nature, 429, 275
Keller, L. P., Wentworth, S. J., McKay, D. S., Taylor, L. A., Pieters, C., & Morris, R. V. 2000, Lunar Planet. Sci. Conf., 31, 1655
Lagerros, J. S. V., Mueller, T. G., Klaas, U., & Erikson, A. 1999, Icarus, 142, 454
Lucke, R. L., Henry, R. C., & Fastie, W. G. 1974, Lunar Planet. Sci. Conf., 5, 469
Marchi, S., Brunetto, R., Magrin, S., Lazzarin, M., & Gandolfi, D. 2005, A&A, 443, 769
Marchi, S., Paolicchi, P., Lazzarin, M., & Magrin, S. 2006, AJ, 131, 1138
McFadden, L. A., Gaffey, M. J., & McCord, T. B. 1984, Icarus, 59, 25
Moroz, L. V., Fisenko, A. V., Semjonova, L. F., Pieters, C. M., & Korotaeva, N. N. 1996, Icarus, 122, 366
Mothe-Diniz, T., Lazzaro, D., Carvano, J. M., & Florczak, M. 2000, Icarus, 148, 494
Murchie, S., & Pieters, C. M. 1996, J. Geophys. Res., 101, 2201
Nathues, A., Mottola, S., Kaasalainen, M., & Neukum, G. 2005, Icarus, 175, 452
Nesvorny, D., Jedicke, R., Whiteley, R. J., & Ivezic, Z. 2005, Icarus, 173, 132
Pieters, C. M., Fischer, E. M., Rode, O., & Basu, A. 1993, J. Geophys. Res., 98, 20817
Pieters, C. M., et al. 2000, Meteoritics Planet. Sci., 35, 1101
Roettger, E. E., & Buratti, B. J. 1994, Icarus, 112, 496
Rottman, G. J., Woods, T. N., & Sparn, T. P. 1993, J. Geophys. Res., 98, 10667
Sasaki, S., Nakamura, K., Hamabe, Y., Kurahashi, E., & Hiroi, T. 2001, Nature, 410, 555
Strazzulla, G., Dotto, E., Binzel, R., Brunetto, R., Barucci, M. A., Blanco, A., & Orofino, V. 2005, Icarus, 174, 31
Taylor, R. C., Birch, P. V., Drummond, J., Pospieszalska-Surdej, A., & Surdej, J. 1987, Icarus, 69, 354
Tedesco, E. F., Noah, P. V., Noah, M., & Price, S. D. 2002, AJ, 123, 1056
Tholen, D. J. 1989, in Asteroids II, ed. R. P. Binzel et al. (Tucson: Univ. Arizona Press), 1139
Vilas, F., & McFadden, L. A. 1992, Icarus, 100, 85
Wagner, J. K., Hapke, B. W., & Wells, E. N. 1987, Icarus, 69, 14
Wamsteker, W., & Gonzelez-Riestra, R. 1998, in Ultraviolet Astrophysics beyond the *IUE* Final Archive, ed. W. Wamsteker & R. Gonzalez Riestra (ESA SP-413; Noordwijk: ESA)
Xu, S., Binzel, R. P., Burbine, T. H., & Bus, S. J. 1995, Icarus, 115, 1
Zellner, B., Tholen, D. J., & Tedesco, E. F. 1985, Icarus, 61, 355